ORIGINAL RESEARCH

Anticancer nanodelivery system with controlled release property based on protocatechuate–zinc layered hydroxide nanohybrid

Farahnaz Barahuie[1]
Mohd Zobir Hussein[1]
Shafinaz Abd Gani[2,3]
Sharida Fakurazi[3,4]
Zulkarnain Zainal[1]

[1]Materials Synthesis and Characterization Laboratory, Institute of Advanced Technology (ITMA), Universiti Putra Malaysia, [2]Department of Biochemistry, Faculty of Biotechnology and Biomolecular Sciences, Universiti Putra Malaysia, [3]Laboratory of Vaccines and Immunotherapeutics, Institute of Bioscience, Universiti Putra Malaysia, [4]Department of Human Anatomy, Faculty of Medicine and Health Sciences, Universiti Putra Malaysia, Serdang, Selangor, Malaysia

Correspondence: Mohd Zobir Hussein
Materials Synthesis and Characterization Laboratory, Institute of Advanced Technology, Block B, Faculty of Engineering, Universiti Putra Malaysia, 43400 UPM, Serdang, Selangor, Malaysia
Tel +603 8946 8092
Fax +603 8946 7006
Email mzobir@upm.edu.my

Background: We characterize a novel nanocomposite that acts as an efficient anticancer agent.

Methods: This nanocomposite consists of zinc layered hydroxide intercalated with protocatechuate (an anionic form of protocatechuic acid), that has been synthesized using a direct method with zinc oxide and protocatechuic acid as precursors.

Results: The resulting protocatechuic acid nanocomposite (PAN) showed a basal spacing of 12.7 Å, indicating that protocatechuate was intercalated in a monolayer arrangement, with an angle of 54° from the Z-axis between the interlayers of the zinc layered hydroxide, and an estimated drug loading of about 35.7%. PAN exhibited the properties of a mesoporous type material, with greatly enhanced thermal stability of protocatechuate as compared to its free counterpart. The presence of protocatechuate in the interlayers of the zinc layered hydroxide was further supported by Fourier transform infrared spectroscopy. Protocatechuate was released from PAN in a slow and sustained manner. This mechanism of release was well represented by a pseudo-second order kinetics model. PAN has shown increased cytotoxicity compared to the free form of protocatechuic acid in all cancer cell lines tested. Tumor growth suppression was extensive, particularly in HepG2 and HT29 cell lines.

Conclusion: PAN is suitable for use as a controlled release formulation, and our in vitro evidence indicates that PAN is an effective anticancer agent. PAN may have potential as a chemotherapeutic drug for human cancer.
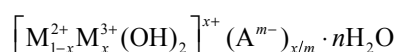
Keywords: protocatechuic acid, nanocomposite, zinc layered hydroxide, zinc oxide, 3T3, HepG2, HeLa, HT29

Introduction

Cancer is a global epidemic, and accounts for more deaths worldwide than other diseases. It affects all ages and socioeconomic groups.

The combination of nanotechnology and medicine, named nanomedicine, has changed the medical world by creating a myriad of new opportunities for advancing the treatment of cancers. Nanoparticles hold the potential to increase the selectivity for eliciting cancer cell death and minimizing toxicity on noncancerous cells.[1,2]
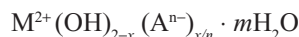
Layered hydroxides such as hydrotalcite-like clays which consist of positively charged layers and exchangeable anions, along with water molecules in the interlayer space, can be classified into two major groups; layered double hydroxides (LDHs) and layered hydroxide salt (LHS). Many successful intercalations have been reported with regards to the use of LDHs as anticancer drug carrier systems.[3–7] LDHs structure has the general formula of:

$$\left[M^{2+}_{1-x} M^{3+}_{x} (OH)_2 \right]^{x+} (A^{m-})_{x/m} \cdot nH_2O$$

where M^{2+} is a divalent metal cation and M^{3+} is a trivalent metal cation; n refers to the number of interlayer water molecules, x represents the layer charge density and A^{m-} is an inorganic or organic interlayer anion with m– charge.[8,9]

Zinc layered hydroxide (ZLH) is an LHS with a general composition of

$$M^{2+}(OH)_{2-x}(A^{n-})_{x/n} \cdot mH_2O$$

where M^{2+} is a metallic cation and A^{n-} represents a counter ion with (n–) charge.[10] ZLHs are currently being used as an additive in concrete,[11] slow release herbicides[12] and drug nanoreservoirs.[13,15] Some anticancer drugs have been intercalated into interlamellae of ZLH, including chlorogenic acid,[13] linoleic acid,[14] ellagic acid,[15] hippuric acid[16] and gallic acid.[17]

The intercalation of protocatechuic acid (Figure 1A) into Mg/AL-LDH has been studied and the resulting material protocatechuate–Mg/Al nanocomposites showed excellent anticancer properties compared to the free drug.[3] However, to the best of our knowledge, application of ZLH as a nanovehicle has yet to be explored and, very little information is available on the use of ZnO as the starting material for the synthesis of nanovehicles for anticancer drug delivery systems.

Zinc is an essential mineral for human health, and is necessary for the function of many enzymes that take part in the synthesis and degradation of lipids, proteins, nucleic acids and carbohydrates in the body. It is also required for the proper function of the immune system.[18,19] In addition, ZLH as a nanocarrier is not stable in low pH medium, and when dissolved in liposomes (pH 4.5–5) it forms zinc anions which are taken up by the body and become part of the nutrient cycle.[20] Furthermore, zinc has excellent antibacterial and antimicrobial properties.[21]

Therefore, here we describe our work on the encapsulation of the protocatechuate anion (Figure 1B) into the interlayers of ZLH through a direct method which is relatively simple, environmentally friendly and economical, as it includes fewer chemicals and steps compared with other layered metal hydroxide synthesis methods like solid state reactions,[22] urea hydrolysis,[23] hydrolysis of salts and oxides[24] and precipitation with alkaline solution.[25]

In the present work, we investigated the properties of the resulting protocatechuate–ZLH intercalation compound by intercalating an anticancer agent, protocatechuate, into the interlayer lamellar host (ZLH). The expected advantages of this approach are high thermal stability, controlled release capability, good solubility in water, and better anticancer efficacy. Furthermore, we selected different types of cancerous cells to evaluate anticancer efficiency on the cancer cells as well as to investigate the possible toxicity induction on the normal fibroblast (3T3) cells.

Materials and methods
Materials
Protocatechuic acid (97%) was obtained from Acros Organics (Geel, Antwerp, Belgium) and was used without further purification. Phosphate-buffered saline (PBS) and ZnO from Sigma-Aldrich (St Louis, MO, USA) were used as received. NaOH was purchased from Friendemann Schmidt (Parkwood, WA, USA) and deionized water was used in all experiments.

Synthesis of ZLH intercalated with protocatechuate
Protocatechuate-ZLH nanocomposite (PAN) was synthesized using ZnO as starting material, by a direct method, similar to previously reported studies.[13,26] About 0.2 g of ZnO was reacted with 100 mL of 0.1 mol/L protocatechuic acid solution. The solution was titrated with l mol/L NaOH to the final pH of 7.9 under vigorous stirring. Then it was aged in an oil bath at 70°C for 18 hours, before being centrifuged and washed with deionized water. The resulting compound was dried in an oven at 60°C overnight.

Characterization
Powder X-ray diffraction patterns were recorded in the range of 2°C–60°C on a Shimadzu diffractometer, XRD-6000 using CuK_α radiation (λ =1.5418 Å) at 30 kV and 30 mA with a dwell time of 4 degrees per minute. Fourier transform
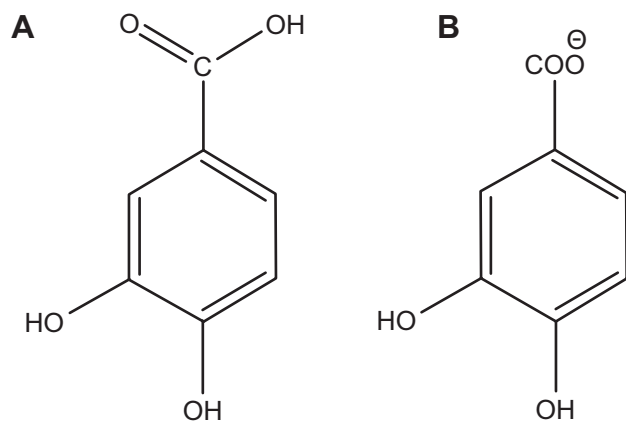

Figure 1 Molecular structure of protocatechuic acid (**A**) and protocatechuic acid anion, protocatechuate (**B**).

infrared (FTIR) spectra of the materials were recorded over the range of 400–4,000 cm^{-1} on a Thermo Nicolet Nexus FTIR (model Smart Orbit) with 4 cm^{-1} resolution, using the KBr disk method. The chemical composition of the samples was analyzed for zinc by inductively coupled plasma atomic emission spectrometry using a Perkin-Elmer spectrophotometer (model Optima 2000 DV) under standard conditions. For carbon, hydrogen, nitrogen and sulfur (CHNS) analyses, a CHNS-932 LECO instrument was used. Thermogravimetric and differential thermogravimetric analyses were carried out using a Mettler Toledo instrument with a heating rate of 10°C per minute in the range of 20°C–1,000°C under nitrogen atmosphere (N$_2$ flow rate 50 mL per minute). Surface characterization of material was carried out using a nitrogen gas adsorption-desorption technique at 77 K, with a Micromeritics ASAP 2000 instrument. A field emission scanning electron microscope (Nova Nanosem 230 model) was used to determine the surface morphology of the samples. Ultraviolet-visible spectra were measured to determine the optical properties, and a controlled release study was performed using a Perkin Elmer ultraviolet (UV)-visible spectrophotometer (Lambda 35).

Loading and release of protocatechuate from PAN

Loading amount of protocatechuate in PAN was determined using a Perkin-Elmer Lambda 35 UV-visible spectrophotometer. About 0.5 mL of 1 mol/L HCl solution and a known amount of PAN were placed in a 10 mL volumetric flask. The concentration of protocatechuate in the solution was measured at 255.8 nm using a standard curve of a series of standard solutions of known protocatechuate concentration. The release of protocatechuate from PAN was performed into a medium of PBS at pH 7.4 and pH 4.8,[27–29] by adding about 28 mg of PAN into 250 mL of the buffer solutions. The accumulated amount of protocatechuate released into the solution was measured at preset time intervals using a spectrophotometer at λ_{max} =255.8 nm. To compare the release rate of protocatechuic acid from PAN with that from the physical mixture of protocatechuic acid and pristine ZLH (prepared for this purpose),[30] the same protocatechuic acid release experiments were performed with 0.40 mg of a physical mixture containing protocatechuic acid (PA) (0.14 mg) and the pristine ZLH (0.26 mg).

Cell culture and MTT cell viability assays

Several cancerous and normal cell lines, including HeLa, HepG2, HT29, and 3T3 cell were grown in Roswell Park Memorial Institute (RPMI) 1640 medium supplemented with 10% fetal bovine albumin, penicillin and streptomycin, and equilibrated with 5% carbon dioxide at 37°C.

An MTT (methylthiazol tetrazolium) based assay was carried out to determine the cell viability. Cells were harvested and seeded in 96-well tissue culture plates at 5.0×10^4 cells/well for 24 hours. PA, PAN and ZnO stock solutions were prepared by dissolving the compound in 1:1 of dimethyl sulfoxide (0.1%) and RPMI. Later the mixture was further diluted in the same media to produce various final concentrations ranging from 0.781–50 µg/mL. Upon attachment, the tested compounds were added until the final volume of 200 µL/well. After 48 hours incubation without shaking, 20 µL of MTT solution (5 mg/mL in PBS) was added in each well and further incubated for 3 hours before being aspirated. Then 100 µL of dimethyl sulfoxide was added per well in order to dissolve the purple formazan salt. The intensity of purple formazan solution, which reflects cell growth was subsequently measured at 570 nm using a microplate reader.

Statistical analysis

All experiments were carried out in triplicates and all the data were presented as the mean ± standard deviation. Statistical differences between measurements were carried out using Student's t-test analysis. Statistical significance was ascertained when $P<0.05$.

Results and discussion
Powder X-ray diffraction and structural model

The Powder X-ray diffraction (PXRD) patterns for ZnO, PAN and protocatechuic acid are given in Figure 2. For ZnO, five intense peaks at 30–60 degrees can be observed which can be associated to diffraction of 100, 002, 101, 102 and 110 planes.[13,31] The diffraction pattern also revealed high crystallinity of ZnO. The formation of protocatechuic acid nanocomposite, PAN is believed to occur through a dissociation-decomposition mechanism in three steps:

1. Hydrolysis of ZnO in the aqueous condition to Zn(OH)$_2$ on the surface of ZnO, to form a layer of Zn(OH)$_2$.

$$ZnO + H_2O \longrightarrow Zn(OH)_2$$

2. Dissociation of the layer and formation of Zn^{2+} species in the presence of acid

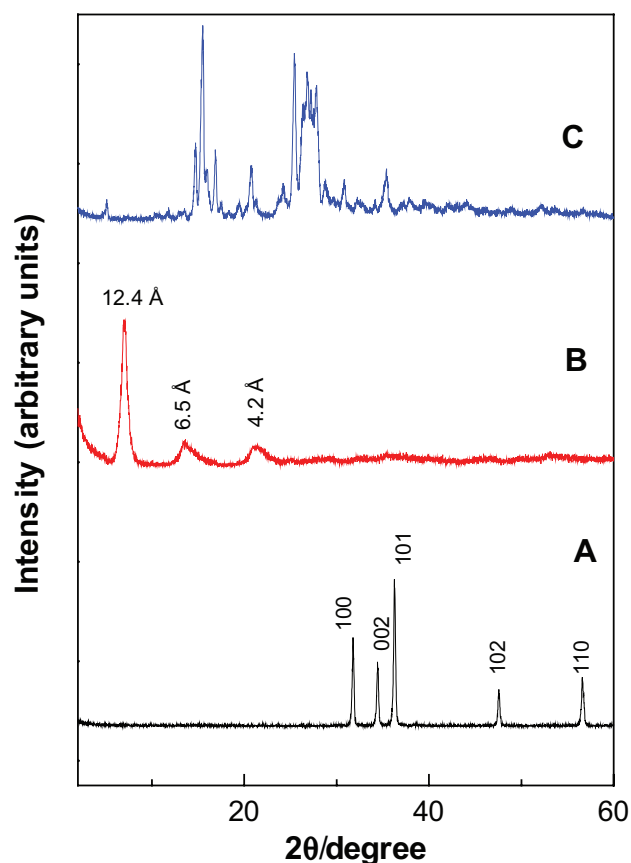$$Zn(OH)_2 \longrightarrow Zn^{2+} + OH^-$$

Figure 2 Powder X-ray diffraction patterns of ZnO (**A**), PAN (**B**) and protocatechuic acid (**C**).
Abbreviation: PAN, protocatechuic acid nanocomposite.

3. The reaction of Zn^{2+} species with protocatechuate anions, hydroxyls and H_2O in the solution to generate the layered PAN nanohybrid compound.[32,33]

$$Zn^{2+} + OH^- + PA^- + H_2O \longrightarrow Zn^{2+}(OH)_{2-x}(PA^{m-})_{x/m} \cdot nH_2O$$

The PXRD of PAN synthesized via direct reaction between PA and ZnO shows an increment in the basal spacing due to the intercalation of protocatechuic acid anions into the ZLH interlayers, as reflected by the observation of peaks at lower 2θ values which was recorded at 7.10, 13.62 and 21.25, with basal spacing of 12.4 Å, 6.5 Å and 4.2 Å, respectively. Disappearance of intense ZnO peaks (Figure 2A) and a protocatechuic acid phase (Figure 2C) also proved that ZnO was successfully converted into ZLH, and at the same time the protocatechuate anion was incorporated into the interlayers of ZLH.

Figure 3A shows the three dimensional molecular size of protocatechuic acid. Using Chem Office software, the long and short axes and molecular thickness of protocatechuic acid were estimated to be 9.0 Å, 6.8 Å and 2.9 Å, respectively (Figure 3A). The average basal spacing of PAN based on three harmonics obtained from X-ray diffraction patterns was estimated to be 12.7 Å, and subtracting the thickness of the ZLH inorganic layers (4.8 Å),[34,35] the expected gallery height for protocatechuate anion occupation was 7.9 Å. This value was smaller than the dimension of protocatechuic acid along the Y-axis, and bigger than the X-axis and the thickness of protocatechuic acid molecule (2.9 Å). Hence, the protocatechuic acid anions have oriented themselves in a monolayer arrangement with an angle of 54 degrees from the Z-axis between the ZLH interlayers, with the carboxylate groups positioned toward the ZLH inorganic layers as shown in Figure 3B.

FTIR spectroscopy

The FTIR spectra for protocatechuic acid and PAN are shown in Figure 4. The FTIR spectrum of protocatechuic
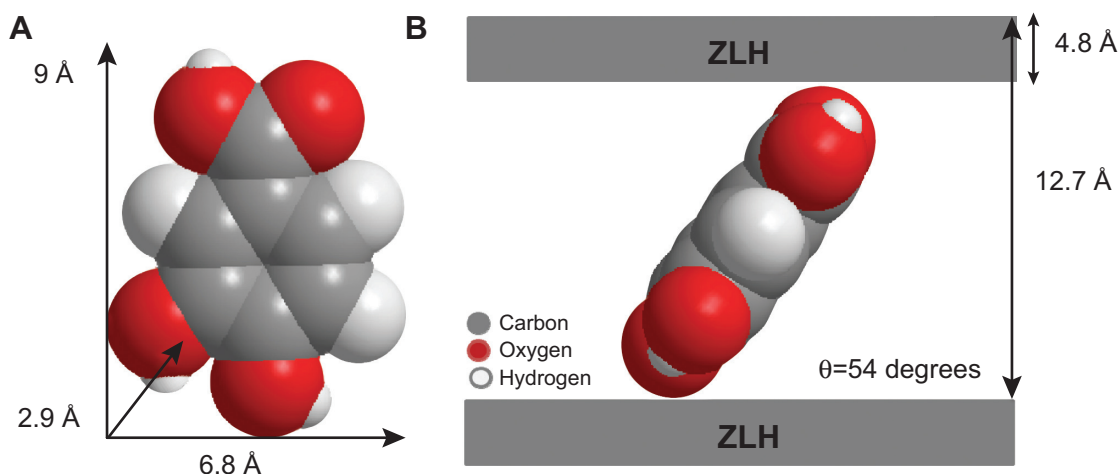

Figure 3 Three-dimensional molecular size of PA (**A**) and spatial orientation of PA intercalated between interlayers of ZLH (**B**).
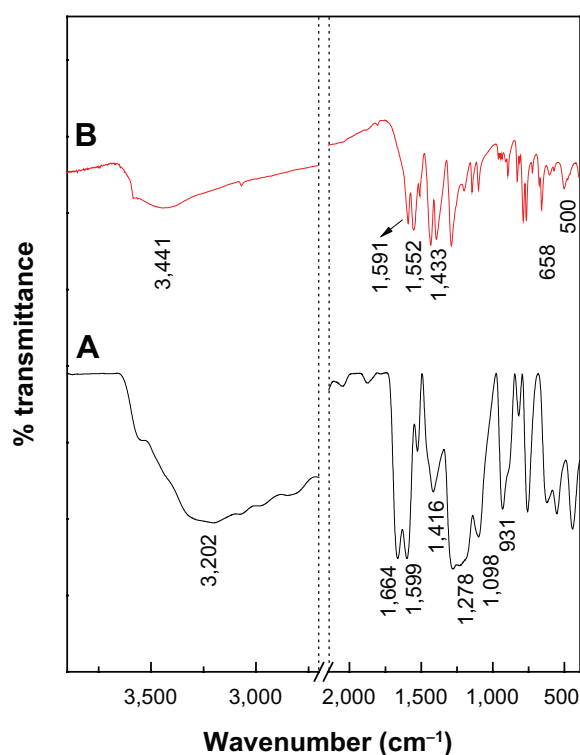**Abbreviations:** PA, protocatechuic acid; ZLH, zinc-layered hydroxide.

Figure 4 Fourier transform infrared spectra of PA (**A**) and PAN (**B**).
Abbreviations: PA, protocatechuic acid; PAN, protocatechuic acid nanocomposite.

acid (Figure 4A) shows a broad absorption peak at 3,202 cm^{-1} due to the OH stretching vibration. The band at 1,664 cm^{-1} can be attributed to the carbonyl functional group in the carboxylic group, while characteristic bands at 1,599 cm^{-1}, 1,526 cm^{-1} and 1,416 cm^{-1} correspond to the C-C stretching of the aromatic ring. C-O stretching bands can be observed at 1,278 cm^{-1} and 1,098 cm^{-1} and the OH bending vibration of the carboxyl group appeared at 931 cm^{-1}.

Figure 4B exhibits some characteristic bands of protocatechuic acid. Although, these vibrations shifted due to the intercalation between protocatechuic acid anions and the interlayer of ZLH, and the peaks at 1,664 cm^{-1} and 931 cm^{-1} were assigned to the C=O stretching and OH bending vibration of carboxyl group have vanished. These observations are taken as supporting evidence for successful intercalation of PA anions into the inorganic layers. The strong absorption band at 3,441 cm^{-1} is attributable to OH stretching vibration, and intense peaks at 1,591 cm^{-1} and 1,393 cm^{-1} are ascribed

to asymmetric and symmetric stretching of the COO$^-$ group, respectively.[36,37] The C-C stretching vibration of the aromatic ring was recorded at 1,552 cm^{-1} and 1,433 cm^{-1}. Furthermore, the adsorption bands at 500 cm^{-1} and 658 cm^{-1} are due to Zn-O and Zn-OH lattice vibrations.[13,38] Successful intercalation of anticancer agent, protocatechuate into interlayer galleries of ZLH was further supported by elemental analysis data as shown in Table 1. The PAN contained 30.2% zinc (weight/weight [w/w]), 19.5% carbon (w/w) and 1.6% hydrogen (w/w) and the loading percentage of protocatechuate in PAN was estimated to be 35.7% (w/w).

Thermal analysis

The thermogravimetric (TGA) and differential thermogravimetric (DTG) measurement of protocatechuic acid and its intercalated compound, PAN, are given in Figure 5. The TGA/DTG thermogram for free protocatechuic acid (Figure 5A) revealed two thermal phenomena. The first step, in the region of 58°C–139°C at maximum temperature of 120°C with 9.2% weight losses, can be associated with the removal of absorbed water. This was followed by a second step of weight loss which occurred in the region of 175°C–303°C, which was attributed to the protocatechuic acid combustion, corresponding to a sharp peak at 254°C with 76.8% mass loss. The decomposition of PAN (Figure 5B) occurred in two major stages. The first one was at around 82°C in the region of 60°C–119°C with weight loss of 4.9%. The second stage was at 587°C in the region 393°C–638°C with 65.7% weight loss. The first step corresponds to removal of surface physisorbed water molecules and the second weight loss associates to the decomposition of incorporated guest anion, protocatechuic acid. It is worth noting that the degradation temperature attributing to PA in the PAN (587°C) is higher than the pure PA decomposition (254°C). This indicates that the thermal stability of the intercalated anticancer agent protocatechuic acid is enhanced because of the intercalation into the ZLH host.

Surface characterization

Figure 6A gives the nitrogen adsorption–desorption isotherms of ZnO and PAN. As can be seen from Figure 6A, the adsorption–desorption isotherm for both precursor and nanocomposite is categorized as Type IV with H3-Type

Table 1 Physicochemical properties of ZnO and PAN

Sample	C (%)	H (%)	Zn (% w/w)	Anion (% w/w)	BET surface area (m²/g)	BJH pore volume (cm³/g)	BJH average pore diameter (Å)
ZnO	–	–	82.7	–	6	0.03	40
PAN	19.5	1.6	30.2	35.7	8	0.04	62

Abbreviations: PAN, protocatechuic acid nanocomposite; w/w, weight/weight; BJH, Barret-Joyner-Halenda method; BET, Brunauer, Emmett and Teller method.
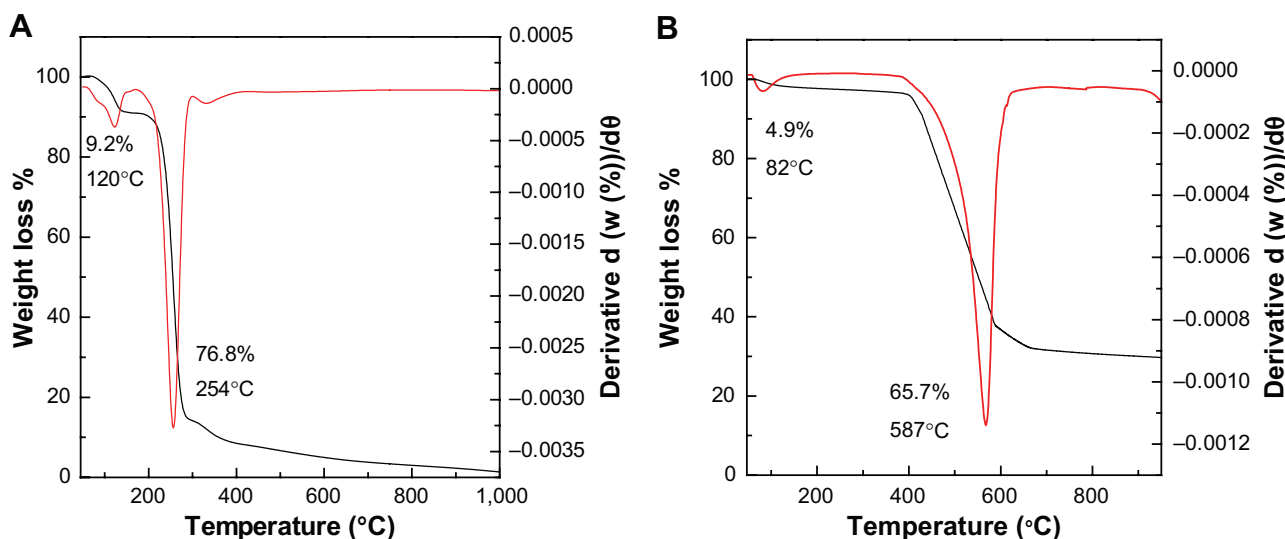
Figure 5 Thermogravimetric and differential thermogravimetric analyses of protocatechuic acid (**A**) and PAN (**B**).
Abbreviation: PAN, protocatechuic acid nanocomposite.

hysteresis loop (by International Union of Pure and Applied Chemistry (IUPAC) classification). This type of loop is typical for materials which have a mesoporous-type structure.[39,40] ZnO showed slow adsorbate uptake at a low relative pressure range of 0.0–0.9. At 0.9, rapid adsorption ensued until an optimum uptake of around 11.2 P/P$_o$ (relative pressure) was achieved. However, the adsorption for PAN occurred in a gradual manner at a relative pressure range of 0.0–0.9, followed by rapid adsorption, and reached a maximum uptake at 29.3 P/P$_o$. The desorption branch of the hysteresis loop for ZnO was much narrower compared to PAN, indicating different pore textures in the precursor and nanocomposite.

The surface area of both materials determined by the Brunauer, Emmett and Teller (BET) method is shown in Table 1. The surface area increased from 6 m^2/g for ZnO to 8 m^2/g for PAN. Furthermore, we recorded an increase in pore size and pore volume from ZnO to PAN. These results confirmed the transformation of ZnO precursor to PAN. As shown in Figure 6B, ZnO gave a single peak pore size distribution at 6.0, 7.7, 12.2, 33.8 and 71.8 Å. On the other hand, a single-peaked pore size distribution was observed for PAN, centered at around 4.6, 6.5, 8.0, 12.6 and 39.0 Å. The average pore diameter and pore volume shown by Barret-Joyner-Halenda (BJH) method desorption are given
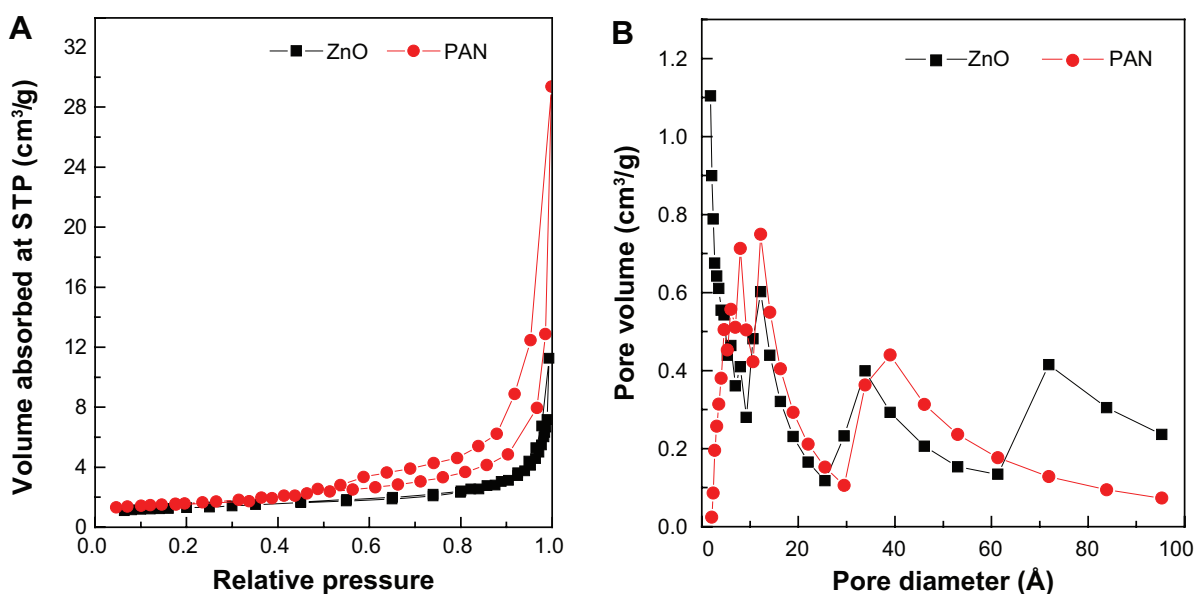

Figure 6 Adsorption-desorption isotherms for ZnO and PAN (**A**), and Barret-Joyner-Halenda method pore size distribution for ZnO and PAN (**B**).
Abbreviations: PAN, protocatechuic acid nanocomposite; STP, standard temperature and pressure.

in Table 1. The BJH average pore diameters for ZnO and PAN were 40 Å and 62 Å, respectively, and the BJH pore volumes for the same samples were 0.03 cm^3/g and 0.04 cm^3/g, respectively.

The surface morphology of ZnO and PAN, examined using a field emission scanning electron microscope (FESEM), is demonstrated in Figure 7. ZnO is shown to have a nonuniform granular structure with various shapes and sizes (Figure 7A and B). As a result of intercalation of protocatechuic acid anions, this structure was converted to an agglomerate of compact and nonporous granular structure (Figure 7C and D).

Transmission electron microscope (TEM) analysis

Figure 8 shows the TEM micrographs of ZnO and PAN. The TEM specimens were prepared by placing a droplet of colloidal solution on a Formvar grid, and drying it in the air. The colloidal solution was obtained by addition of a known amount of ZnO/nanocomposite into 5 mL of solvent (50% acetone, 50% deionized water), and then sonicated for 30 minutes. The small rod-like shaped particles of length 123 nm and diameter 65 nm for ZnO (Figure 8A) changed upon the intercalation of protocatechuic acid into the inorganic host, to the roughly spherical shape with the average size of 46 nm in PAN (Figure 8B).

Release behavior of protocatechuate anions

To investigate the release behavior of protocatechuic acid from PAN and its physical mixture, the samples were individually dispersed into PBS at pH 7.4 and pH 4.8. Figure 9B provides the release profiles of PAN at pH 7.4 and pH 4.8, and
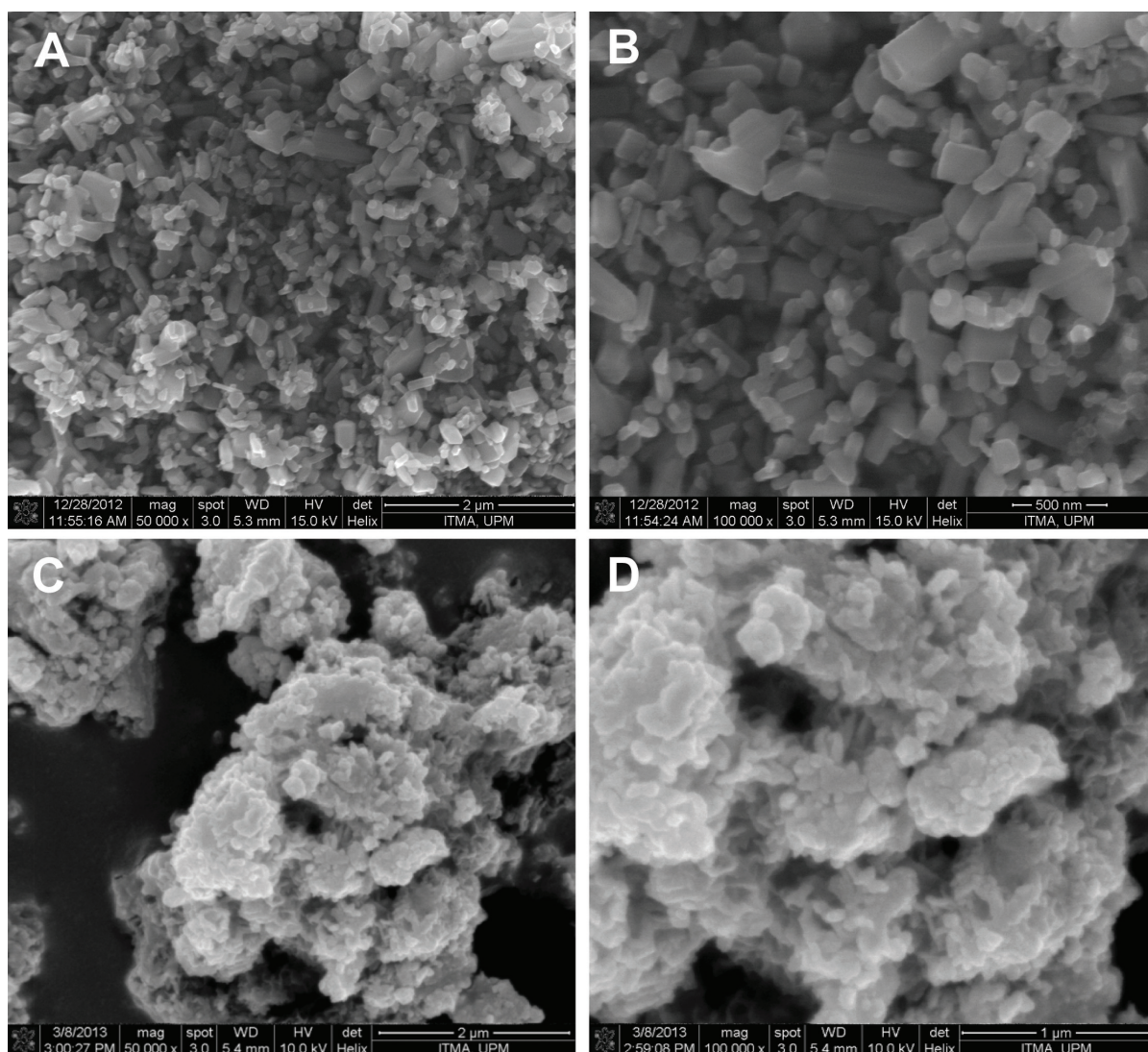

Figure 7 Field emission scanning electron micrograph of ZnO (at 50,000× [**A**] and 100,000× [**B**]) and protocatechuic acid nanocomposite (at 50,000× [**C**] and 100,000× [**D**]).
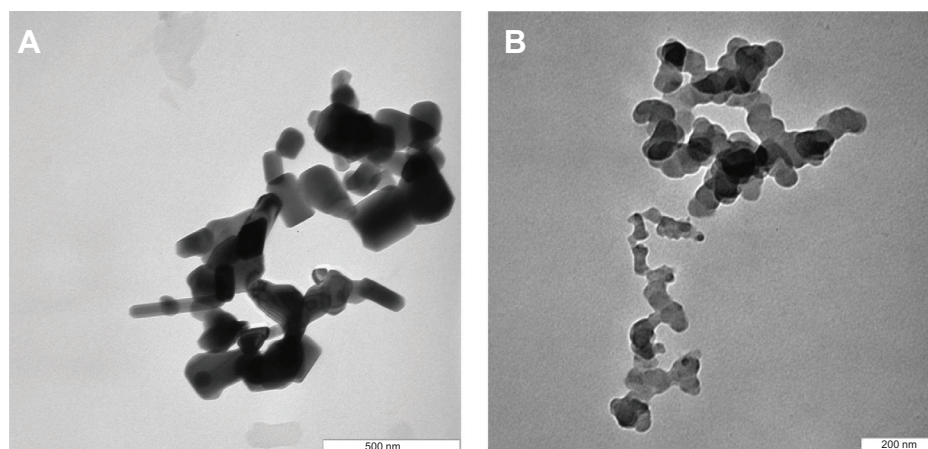
Figure 8 TEM images of ZnO (**A**), and PAN (**B**).
Abbreviations: TEM, transmission electron microscope; PAN, protocatechuic acid nanocomposite.

the release profiles of a physical mixture of protocatechuic acid with ZnO into PBS at pH 7.4 and pH 4.8 media are shown in Figure 9A. The free protocatechuic acid released quickly, and the release was completed within 10 minutes in both pH 7.4 and pH 4.8 PBS, indicating that the interaction between the contents of the physical mixture was almost negligible. On the other hand, the release of protocatechuic acid from PAN was obviously much slower than that from the physical mixture. This phenomena is ascribed to the electrostatic attraction between protocatechuate anions and the ZLH inorganic layers together with the ion-exchange property, and these results revealed the novelty of ZLH being used in a controlled release formulation of an anticancer drug, protocatechuic acid.

Figure 9B clearly displays that the pH value of the medium imposes an influence on the release performance

of protocatechuic acid anions from the PAN nanocomposite. The release rate at pH 7.4 was remarkably lower than that at pH 4.8, whereas the release percentage of protocatechuic acid from PAN at pH 7.4 was about 87% within 7,001 minutes, compared to 95% within 1,592 minutes at pH 4.8. Furthermore, the release profile of the nanocomposite at pH 4.8 for the first 372 minutes showed a fast release with 76%, which is possibly attributed to partial dissolution of the ZLH layers because of the instability of ZLH in acidic media. It was followed by a slower step which is related to the ion-exchange process between the protocatechuate anion pillared into the lamella host and the phosphate anions in the buffer solution.[41–43] However, ZLH is stable in a pH 7.4 environment and the mechanism of the modified drug release in this media may have occurred through an ion-exchange reaction between the drug anions
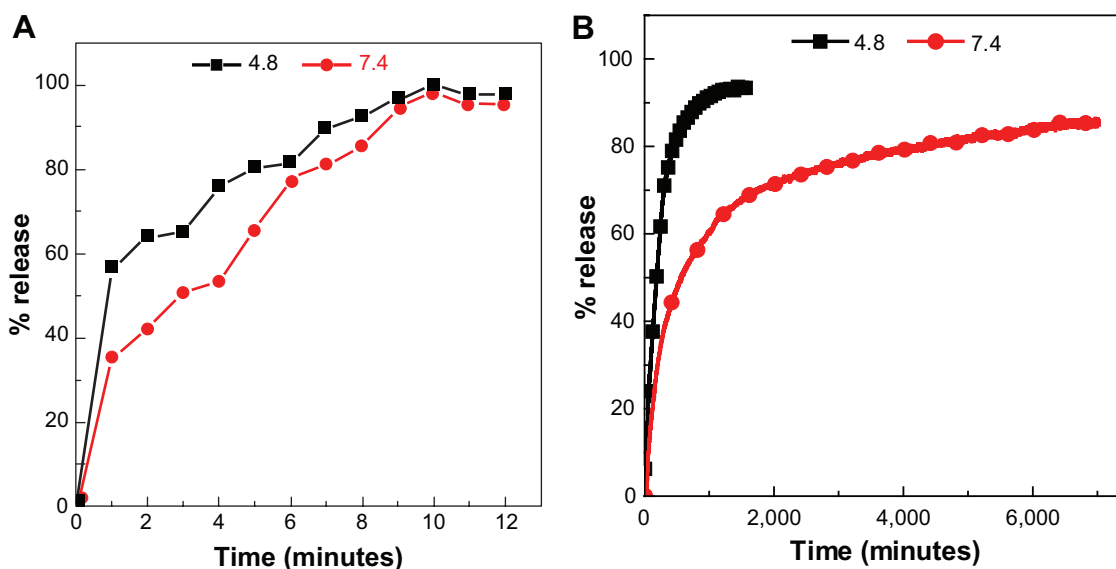

Figure 9 Release profiles of a physical mixture of protocatechuic acid with zinc layered hydroxide at pH 7.4 and pH 4.8 (**A**) and release profiles of protocatechuate from protocatechuic acid nanocomposite at pH 7.4 and pH 4.8 (**B**).

Table 2 Correlation coefficient (R^2), rate constants (k), and half life ($t_{1/2}$) values obtained by fitting the data of the release of PA from PAN into phosphate-buffered saline at pH 4.8 and 7.4

Aqueous solution	Saturation release (%)	R^2			Pseudo-second order	
		Pseudo-first order	Pseudo-second order	Parabolic diffusion	Rate constant, K (g/mg·h)	$t_{1/2}$(h)
pH 7.4	87	0.9694	0.9962	0.8354	2.07×10^{-5}	531
pH 4.8	95	0.9686	0.9966	0.8018	5.86×10^{-5}	162

Abbreviations: PAN, protocatechuic acid nanocomposite; PA, protocatechuic acid.

and the phosphate buffer anions.[41–43] The release behavior of protocatechuic acid demonstrates a similar result to other drugs such as chlorogenic acid[13] and perindopril erbumine,[44] found in the literature.

Release kinetics of protocatechuate from PAN

Kinetic release of protocatechuate from PAN was analyzed using various kinetic models, namely the pseudo–first order (Equation 1),[45] pseudo–second order (Equation 2),[46] and parabolic diffusion (Equation 3)[47] equations:

$$\ln(q_e - q_t) = \ln q_e - k_1 t \qquad (1)$$

$$t/q_t = 1/k_2\, q_e^2 + t/q_e \qquad (2)$$

$$(1 - M_t/M_o)/t = kt^{-0.5} + b \qquad (3)$$

where M_o and M_t are the amount of protocatechuic acid between the layers at release time 0 and t, respectively; q_e and q_t are the amount of protocatechuic acid released at equilibrium and at time t, respectively; k is the corresponding release rate constant, and b is a constant.

For three kinetic models, the plots are represented in Figure 10A–F. As evident with the values of correlation coefficient, R^2 in Table 2, the pseudo–second order kinetic was the best fit for release of protocatechuic acid anion from ZLH interlayers. This result is similar to the kinetic study for the release of chlorogenic acid from ZLH layers,[13] camptothecin from Mg/Al-LDH,[46] and cetirizine from ZLH.[48] The correlation coefficient and release rate constant at pH 4.8 (Figure 10E) are 0.9966 and 5.86×10^{-5} g/mg·h respectively, compared with 0.9962 and 2.07×10^{-5} g/mg·h, respectively at pH 7.4 (Figure 10B).

Cytotoxicity assay of PAN, protocatechuic acid and ZnO samples against 3T3, HeLa, HepG2 and HT29 cell lines

The efficacy of PAN, PA, and ZnO in suppressing the growth of HeLa cervical adenocarcinoma, HT29 colorectal adenocarcinoma and HepG2 liver hepatocarcinoma was assessed using a colorimetric assay (MTT assay) as various cell lines possessed different sensitivity toward drugs. The 3T3 normal fibroblast cells were employed as a respective control.

PA and PAN demonstrated growth inhibition against all tested cancerous cell lines including HeLa, HepG2 and HT29 cells. As illustrated in Figure 11, HeLa, HepG2 and HT29 cells displayed a dose-dependent reduction in cell viability after 48 hours of incubation. These two drugs exerted a cytotoxic effect on all tested cell lines at higher concentrations ($>$25 μg/mL), and showed a slight toxicity at lower concentrations.

In general, PA exhibited a much lower cytotoxic effect on the cancerous cells with a higher half maximal inhibitory concentration value (IC_{50}) compared to the IC_{50} value of PAN as presented in Table 3. Interestingly, a higher PAN cytotoxicity was demonstrated in HepG2 and HT29 cells. PAN decreased cell viability of HepG2, with an IC_{50} of 20.5 μg/mLwhen compared to PA which was 41 μg/mL. The same goes for HT29, where the IC_{50} of PAN was found to be 24.5 μg/mL. This value was much lower compared to the IC_{50} of PA, which was 46.5 μg/mL. By contrast, the lowest cytotoxicity was observed in the HeLa cell line, where the calculated IC_{50} was around 36 μg/mL. However, the IC_{50} value of PAN was not significant from the IC_{50} value of PA, which was 40 μg/mL. This shows that the introduction of the ZnO layer into PA improved the efficacy of PA in HepG2 and HT29 cell lines.

It is apparent from Figure 11 that both PA and PAN did not induce toxicity in 3T3 cells. Both compounds did not affect cell viability in the tested range, as the survival was consistently greater than 70% or similar to control. In this case, it can be suggested that both PA and PAN possessed good anticancer activities and demonstrated selectivity between cancerous and normal cells.

Figure 11 shows that upon exposure to $<$25 μg/mL ZnO, there was no significant inhibition in cell proliferation in all four cell lines tested. However, increasing ZnO concentration led to death of these cells. At 50 μg/mL, the cell viability was 34.5%, 40%, 47% and 44.5%
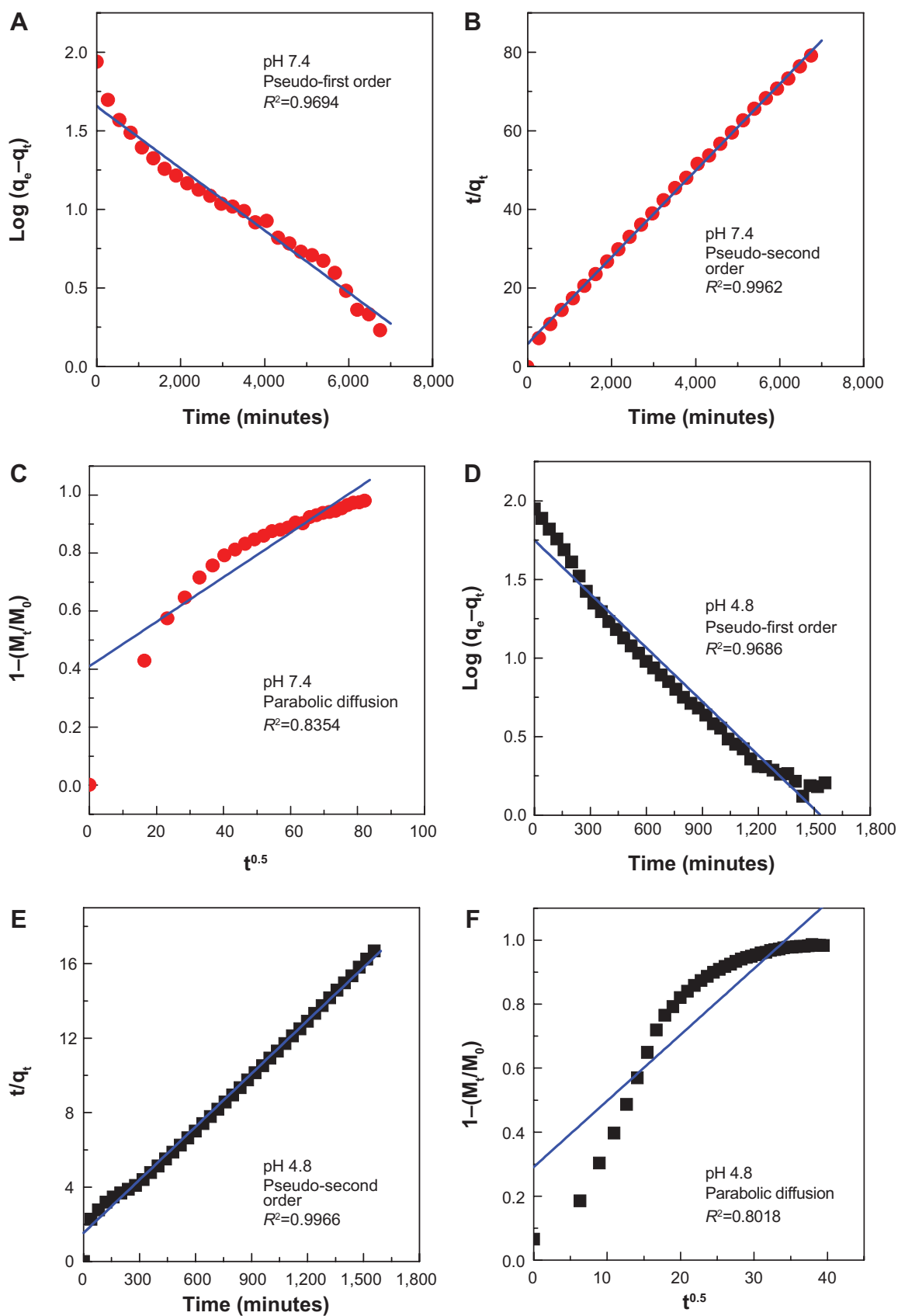
Figure 10 Fitting of the data for PA release from PAN into various solutions to the pseudo-first order, pseudo-second order kinetics and parabolic diffusion model for pH 7.4 (**A**–**C**) and pH 4.8 (**D**–**F**).
Abbreviations: PA, protocatechuic acid; PAN, protocatechuic acid nanocomposite; M_0, amount of protocatechuic acid between the layers at release time 0; Mt, amount of protocatechuic acid between the layers at release time t; qe, amount of protocatechuic acid released at equilibrium; qt, amount of protocatechuic acid released at time t; k, release rate constant.

Table 3 The half maximal inhibitory concentration (IC$_{50}$) value for PA, PAN and ZnO samples tested on 3T3, HeLa, HepG2 and HT29 cell lines

Cell type	IC$_{50}$ (µg/mL)		
	PA	**PAN**	**ZnO**
3T3	No cytotoxicity	No cytotoxicity	44.5
HeLa	40.0	36.0	34.5
HepG2	41.0	20.5	40.0
HT29	46.5	24.5	47.0

Note: Values are in µg/mL.
Abbreviations: PAN, protocatechuic acid nanocomposite; PA, protocatechuic acid.

for HeLa, HepG2, HT29 and 3T3, respectively. This shows that in vitro, ZnO has a cytotoxic ability to suppress the growth of both cancerous and normal cells without a selective manner.

In contrast, it has been reported that ZnO nanoparticles selectively induce apoptosis in cancerous cells, while posing no negative impact on normal cells. Even so, in their studies, all the tested cell lines were exposed to a low concentration of ZnO, which was only up to 15 µg/mL for 24 hours, which was much lower than the concentration tested in this study.[49]

The toxicity of ZnO toward normal cells and cancerous cells is strongly related to the intracellular dissolution of ZnO to ionic Zn^{2+}.[50] Despite that, there is an argument as to whether the toxicity toward these cells was attributed solely to released ionic Zn^{2+}, or the non-dissolved particle of ZnO, or the combination of these two processes.[51,52] This will induce oxidative stress, DNA damage and eventually cell death via apoptosis.[53]
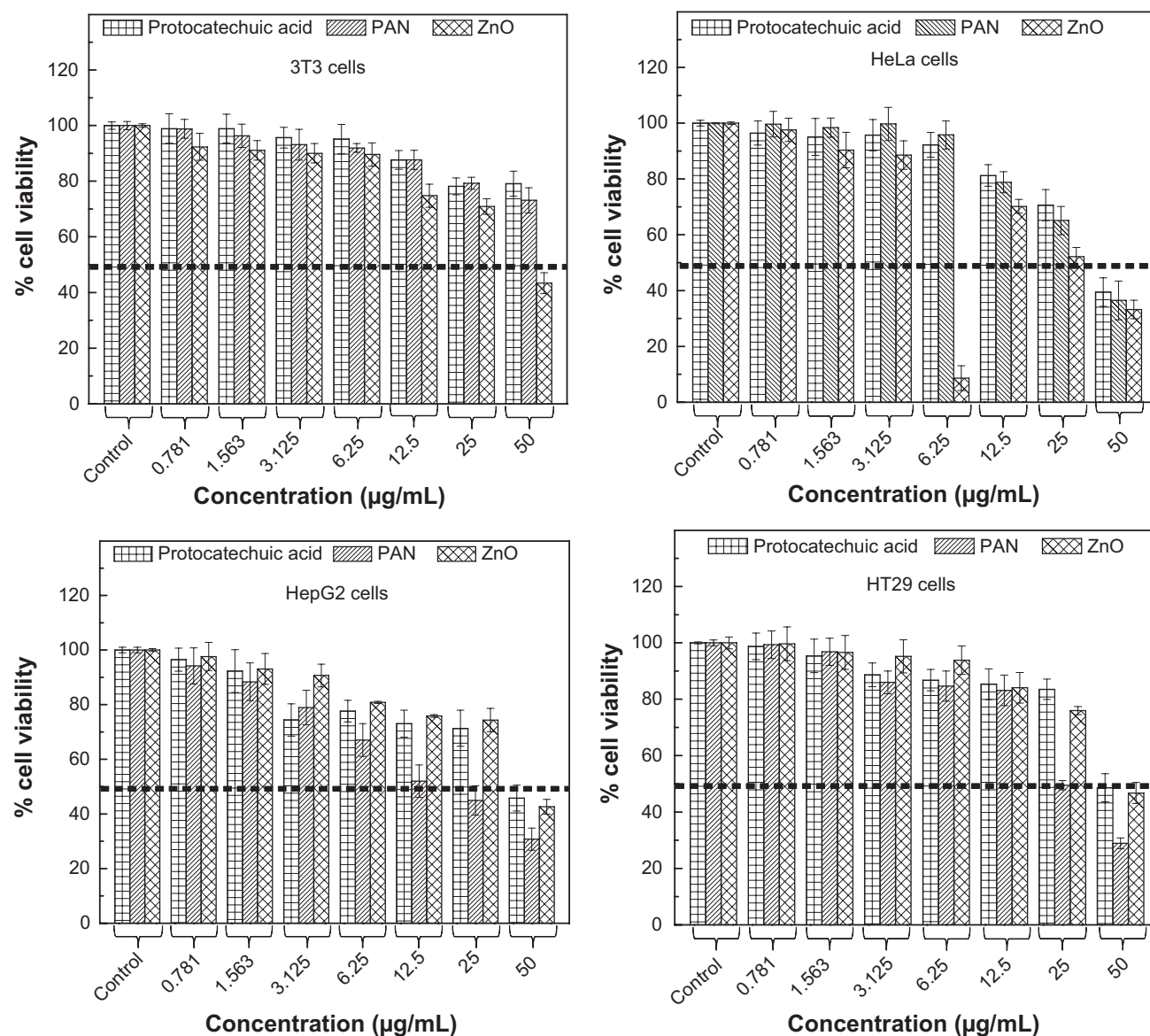

Figure 11 Cell viability (MTT assay) of 3T3, HeLa, HepG2 and HT29 cell lines exposed to various gradient concentrations.
Note: The data presented are mean ± standard deviation of triplicate values.
Abbreviations: PAN, protocatechuic acid nanocomposite; MTT, methylthiazol tetrazolium.

In order to prevent the cytotoxic effect of ZnO, further investigation is required. Previous studies regarding this matter focused on the coating of ZnO nanoparticles with nontoxic, naturally occurring or synthetic polymers, such as starch and polyethylene glycol, to greatly protect the normal cells from the toxicity effects of ZnO nanoparticles.[54]

Conclusion

In the present work, the intercalation of a drug active, protocatechuic acid into the ZLH interlayer spaces was accomplished using ZnO as a precursor to generate PAN. A relatively high loading percentage of protocatechuate of about 35.7% and FTIR analysis together with X-ray diffraction studies supported the intercalation between the protocatechuate moiety and the positive charge of ZLH inorganic interlayers. X-ray diffraction patterns suggested an expansion of interlayer spacing to 12.7 Å due to the monolayer arrangement of protocatechuate anions with the angle of 54 degrees from the Z-axis. The release study showed that about 95% of the guest protocatechuate could be released in 1,592 minutes in pH 4.8 PBS compared to 87% in 7,001 minutes at pH 7.4, with the release governed by pseudo-second order kinetics. Furthermore, the guest anion, protocatechuate, was thermally more stable than its unbound counterpart. In essence, the introduction of ZLH for the intercalation of PA improved the anticancer efficacy and selectivity features of the resulting compound. After 48 hours of treatment, the highest growth suppression and IC_{50} value was much more prominent in both HepG2 and HT29 cell lines. These features suggest great potential for PAN as a novel alternative for chemopreventive and chemotherapeutic treatments in human cancer. However, for the development of cancer treatment regimes, the concentration of the nanocarrier system needs to be in the safe therapeutic range, as higher concentrations of ZnO will kill not only cancerous cells, but also noncancerous cells. Future studies should be performed in order to further the understanding of this cytotoxicity mechanism in depth.

Acknowledgments

Disclosure

The authors have no conflicts of interest in this work.

References

1. Riaz U, Ashraf SM. Double layered hydroxides as potential anti-cancer drug delivery agents. *Mini Rev Med Chem*. 2013;13(4):522–529.
2. Gmeiner WH, Ghosh S. Nanotechnology for cancer treatment. *Nanotechnology Reviews*. 2013:1–13.
3. Barahuie F, Hussein MZ, Hussein-Al-Ali SH, Arulselvan P, Fakurazi S, Zainal Z. Preparation and controlled-release studies of protocatechuic acid-magnesium/aluminium-layered double hydroxide nanocomposite. *Int J Nanomedicine*. 2013;8:1975–1987.
4. Qin L, Wang M, Zhu R, You S, Zhou P, Wang S. The in vitro sustained release profile and antitumor effect of etoposide-layered double hydroxide nanohybrids. *Int J Nanomedicine*. 2013;8:2053–2064.
5. Chakraborty J, Roychowdhury S, Sengupta S, Ghosh S. Mg-Al layered double hydroxide-methotrexate nanohybrid drug delivery system: evaluation of efficacy. *Materials Science and Engineering C*. 2013;33(4):2168–2174.
6. Jin L, Liu Q, Sun Z, Ni X, Wei M. Preparation of 5-Fluorouracil/-Cyclodextrin Complex Intercalated in Layered Double Hydroxide and the Controlled Drug Release Properties. *Ind Eng Chem Res*. 2010;49:11176–11181.
7. Li F, Jin L, Han J, Wei M, Li C. Synthesis and Controlled Release Properties of Prednisone Intercalated Mg-Al Layered Double Hydroxide Composite. *Ind Eng Chem Res*. 2009;48:5590–5597.
8. Seida Y, Nakano Y. Removal of phosphate by layered double hydroxides containing iron. *Water Res*. 2002;36(5):1306–1312.
9. Kwon SJ, Choy JH. A novel hybrid of Bi-based high-Tc superconductor and molecular complex. *Inorg Chem*. 2003;42(25):8134–8136.
10. Arizaga GGC, Satyanarayana KG, Wypych F. Layered hydroxide salts: Synthesis, properties and potential applications. *Solid State Ion*. 2007; 178:1143–1162.
11. Arefi MR, Rezaei-Zarchi S. Synthesis of Zinc Oxide Nanoparticles and Their Effect on the Compressive Strength and Setting Time of Self-Compacted Concrete Paste as Cementitious Composites. *Int J Mol Sci*. 2012;13(4):4340–4350.
12. Hussein MZ, Rahman NS, Sarijo SH, Zainal Z. Herbicide-intercalated zinc layered hydroxide nanohybrid for a dual-guest controlled release formulation. *Int J Mol Sci*. 2012;13:7328–7342.
13. Barahuie F, Hussein MZ, Arulselvan P, Fakurazi S, Zainal Z. Development of the anticancer potential of a chlorogenate-zinc layered hydroxide nanohybrid with controlled release property against various cancer cells. *Sci Adv Mater*. 2013;5:1983–1993.
14. Choy JH, Shin J, Lim SY, Oh JM, Oh MH, Oh H. Characterization and stability analysis of ZnO nanoencapsulated conjugated linoleic acid. *J Food Sci*. 2010;75(6):N63–N68.
15. Hussein MZ, Al Ali SH, Zainal Z, Hakim MN. Development of antiproliferative nanohybrid compound with controlled release property using ellagic acid as the active agent. *Int J Nanomedicine*. 2011;6:1373–1383.
16. Hussein Al Ali SH, Al-Qubaisi M, Hussein MZ, Zainal Z, Hakim MN. Preparation of hippurate-zinc layered hydroxide nanohybrid and its synergistic effect with tamoxifen on HepG2 cell lines. *Int J Nanomedicine*. 2011;6:3099–3111.
17. Hussein MZ, Ghotbi MY, Yahaya AH, Rahman MZ. Synthesis and characterization of (zinc-layered-gallate) nanohybrid using structural memory effect. *Mater Chem Phys*. 2009;113:491–496.
18. Jeejeebhoy K. Zinc: An Essential Trace Element for Parenteral Nutrition. *Gastroenterology*. 2009;137(5):S7–S12.
19. Leggett RW. A biokinetic model for zinc for use in radiation protection. *Sci Total Environ*. 2012;420:1–12.
20. Xia SJ, Ni ZM, Xu Q, Hu BX, Hu J. Layered double hydroxides as supports for intercalation and sustained release of antihypertensive drugs. *J Solid State Chem*. 2008;181(10):2610–2619.
21. Faiz U, Butt T, Satti L, Hussain W, Hanif F. Efficacy of zinc as an antibacterial agent against enteric bacterial pathogens. *J Ayub Med Coll Abbottabad*. 2011;23(2):18–21.
22. Rajamathi M, Kamathi PV. Urea hydrolysis of cobalt(II) nitrate melts: synthesis of novel hydroxides and hydroxynitrates. *Inter J Inorg Mater*. 2001;7:901–906.

23. Stählin W, Oswald HR. The crystal structure of zinc hydroxide nitrate, $Zn_5(OH)_8(NO_3)_2.2H_2O$. *Acta Crystallogr Sect B*. 1970;26:860–863.

24. Rouba S, Rabu P, Drillon M. Synthesis and characterization of new quasione-dimensional Mn(II) hydroxynitrates (MnxZn1-x)(OH)(NO3) H2O(x=0.53, 1.00). *J Solid State Chem*. 1995;118:28–32.

25. Cursino ACT, Mangrich AS, Da Costa Gardolinski JEF, Mattoso N, Wypych F. Effect of confinement of anionic organic ultraviolet ray absorbers into two-dimensional zinc hydroxide galleries. *J Braz Chem Soc*. 2011;22:1183–1191.

26. Hussein Al Ali S, Al-Qubaisi M, Hussein MZ, Ismail M, Zainal Z, Hakim MN. Controlled-release formulation of antihistamine based on cetirizine zinc-layered hydroxide nanocomposites and its effect on histamine release from basophilic leukemia (RBL-2H3) cells. *Int J Nanomedicine*. 2012;7:3351–3363.

27. Xia SJ, Ni ZM, Xu Q, Hu BX, Hu J. Layered double hydroxides as supports for intercalation and sustained release of antihypertensive drugs. *J Solid State Chem*. 2008;181(10):2610–2619.

28. Ribeiro C, Arizaga GG, Wypych F, Sierakowski MR. Nanocomposites coated with xyloglucan for drug delivery: In vitro studies. *Int J Pharm*. 2009;367(1–2):204–210.

29. Hussein MZ, Hashim N, Yahaya AH, Zainal Z. Synthesis and characterization of [4-(2,4-dichlorophenoxybutyrate)-zinc layered hydroxide] nanohybrid. *Solid State Sci*. 2010;12(5):770–775.

30. Newman SP, Jones W. Comparative study of some layered hydroxide salts containing exchangeable interlayer anions. *J Solid State Chem*. 1999;148(1):26–40.

31. Fernandes DM, Silva R, Winkler Heichenletner AA, et al. Synthesis and characterization of ZnO, CuO and a mixed Zn and Cu oxide. *Mater Chem Phys*. 2009;115:110–115.

32. Degen A, Kosec M. Effect of pH and impurities on the surface charge of zinc oxide in aqueous solution. *J Eur Ceram Soc*. 2000;20:667–673.

33. Xingfu Z, Zhaolin H, Yiqun F, Su C, Weiping D, Nanping X. Microspheric organization of multilayered ZnO nanosheets with hierarchically porous structures. *J Phys Chem C*. 2008;112:11722–11728.

34. Misra C, Perrota AJ. Composition and properties of synthetic hydrotalcites. *Clays Clay Miner*. 1992;40:145–150.

35. Hwang SH, Han YS, Choy JH. Intercalation of functional organic molecules with pharmaceutical, cosmeceutical and nutraceutical functions into layered double hydroxides and zinc basic salts. *Bull Korean Chem Soc*. 2001;22:1019–1022.

36. Refat MS, Teleb SM, Sadeek SA, Khater HM, El-Megharbel SM. Synthesis and characterization of some hippurato rare earth metal complexes. *J Korean Chem Soc*. 2005;49(3):261–268.

37. Brzyska W, Hakim M. Thermal decomposition of Y, La and light lanthanide complexes of hippuric acid. *J Therm Anal Calorim*. 1988;34(1):47–53.

38. Wang Z, Wang E, Gao L, Xu L. Synthesis and properties of Mg2Al layered double hydroxides containing 5-fluorouracil. *J Solid State Chem*. 2005;178(3):736–741.

39. Sing KSW. The use of gas adsorption for the characterization of porous solids. *J Colloid Interface Sci*. 1989;38:113–124.

40. Zhi Y, Li Y, Zhang Q, Wang H. ZnO nanoparticles immobilized on flaky layered double hydroxides as photocatalysts with enhanced adsorptivity for removal of acid red G. *Langmuir*. 2010;26:15546–15553.

41. Zhang H, Zou K, Sun H, Duan X. A magnetic organic-inorganic composite: Synthesis and characterization of magnetic 5-aminosalicylic acid intercalated layered double hydroxides. *J Solid State Chem*. 2005;178:3485–3493.

42. Ambrogi V, Fardella G, Grandolini G, Perioli L, Tiralti MC. Intercalation compounds of hydrotalcite-like anionic clays with anti-inflammatory agents, II: uptake of diclofenac for a controlled release formulation. *AAPS Pharm Sci Tech*. 2002;3:77–82.

43. Hussein MZ, Zainal Z, Yahaya AH, Foo DWV. Controlled release of a plant growth regulator, alpha-naphthalene acetate from the lamella of Zn-Al-layered double hydroxide nanocomposite. *J Control Release*. 2002;82:417–427.

44. Al Ali SHH, Al-Qubaisi M, Hussein MZ, Ismail M, Zainal Z, Hakim MN. Comparative study of Mg/Al- and Zn/Al-layered double hydroxide-perindopril erbumine nanocomposites for inhibition of angiotensin-converting enzyme. *Int J Nanomedicine*. 2012;7:4251–4262.

45. Liu C, Hou W, Li L, Li Y, Liu S. Synthesis and characterization of 5-fluorocytosine intercalated Zn-Al layered double hydroxide. *J Solid State Chem*. 2008;181(8):1792–1797.

46. Dong L, Yan L, Hou WG, Liu SJ. Synthesis and release behavior of composites of camptothecin and layered double hydroxide. *J Solid State Chem*. 2010;183(8):1811–1816.

47. Ho YS, Ofomaja AE. Pseudo-second-order model for lead ion sorption from aqueous solutions onto palm kernel fiber. *J Hazard Mater*. 2006;129(1–3):137–142.

48. Hussein Al Ali SHH, Al-Qubaisi M, Hussein MZ, Ismail M, Zainal Z, Hakim MN. Controlled-release formulation of antihistamine based on cetirizine zinc-layered hydroxide nanocomposites and its effect on histamine release from basophilic leukemia (RBL-2H3) cells. *Int J Nanomedicine*. 2012;7:3351–3363.

49. Akhtar MJ, Ahamed M, Kumar S, Khan MMA, Ahmad J, Alrokayan SA. Zinc oxide nanoparticles selectively induce apoptosis in human cancer cells through reactive oxygen species. *Int J Nanomedicine*. 2012;7:845–857.

50. Xia T, Kovochich M, Liong M, et al. Comparison of The Mechanism of Toxicity of Zinc Oxide and Cerium Oxide Nanoparticles Based on Dissolution and Oxidative Stress Properties. *ACS Nano*. 2008;2:2121–2134.

51. Cho WS, Duffin RS, Howie E, Scotton CJ, Wallace WA, MacNee W. Progressive Severe Lung Injury By Zinc Oxide Nanoparticles: The Role of Zn^{2+} Dissolutioninside Lysosomes. *Particle and Fibre Toxicol*. 2011;8:27–43.

52. Zhang J, Song W, Guo J, et al. Toxic Effect of Different Zno Particles on Mouse Alveolar Macrophages. *J Hazard Mater*. 2012;219–220:148–155.

53. Xia T, Kovochich M, Brant J, et al. Comparison of the abilities of mbient and manufactured nanoparticles to induce cellular toxicity according to an oxidative stress paradigm. *Nano Lett*. 2006;6:1794–1807.

54. Colon G, Ward BC, Webster TJ. Increased Osteoblast and Decreased Staphylococcus Epidermidis Functions on Nanophase ZnO and TiO. *J Biomed Mater Res*. 2006;78:595–599.